Linear Meta-Model optimization for regional climate models (LiMMo version 1.0)

Sergei Petrov[1], Andreas Will[2], and Beate Geyer[1]

[1]Institute of Coastal Systems, Helmholtz-Zentrum Hereon, Germany
[2]Atmospheric Processes, BTU Cottbus-Senftenberg, Germany

Correspondence: Sergei Petrov (sergei.petrov@hereon.de)

Abstract. A new tool for objective parameter tuning of regional climate models is presented. The climate model output was emulated using a linear regression approach for each grid point on a monthly mean basis. This linear approximation showed decent accuracy over a 6-year period. The root-mean-square error norm between the Meta-Model and the observational data sets was minimized using the gradient-based, limited-memory Broyden-Fletcher-Goldfarb-Shanno method with box constraints.

5   We refer to this framework as LiMMo (Linear Meta-Model optimization). The LiMMo framework was applied to the state-of-the-art regional climate model ICON-CLM, tuned to the E-OBS and HOAPS observational data sets. Different optimization objectives were explored by assigning varying weights to model variables in the error norm definition. The combination of a linear emulator with fast gradient-based optimization allows the proposed method to scale linearly with the number of model variables and parameters, facilitating the tuning of dozens of parameters simultaneously.

1 Introduction

Tuning model parameters is crucial in Earth system modeling, where the aim is to minimize discrepancies between simulation results and observations. This process is essential for achieving reliable simulations in a variety of applications, ranging from short-term numerical weather prediction (e.g., Zängl, 2023) to long-term global and regional climate projections (e.g., Mauritsen and Roeckner, 2020). As model complexity and resolution continue to grow, tuning becomes increasingly challenging due to the computational expense of each simulation, therefore the demand for robust, transparent and efficient tuning procedures has grown significantly. Effective tuning improves model fidelity and enhances trust in model outcomes for policy-relevant decision-making.

In the context of global and regional climate models, four primary approaches to tuning have emerged (Hourdin et al., 2017). The first and most widely used is **expert tuning**, where model developers or users manually adjust parameters based on empirical experience and trial-and-error procedures (e.g., Mauritsen et al., 2012; Golaz et al., 2013). A more systematic alternative is metamodel-based tuning, also known as **objective calibration**, where a computationally cheap surrogate parameterized model (emulator) is constructed to approximate the behavior of the full model (e.g., Neelin et al., 2010; Bellprat et al., 2012). Third, **Bayesian frameworks** explicitly incorporate observational uncertainty and prior knowledge to estimate probability distributions of parameter values (see Kennedy and O'Hagan, 2001; Hourdin et al., 2023). Lastly, **resolution-linked hierarchical**

emulators combine outputs from low- and high-resolution models to reduce computational burden while retaining accuracy (Williamson et al., 2012). This study contributes to the second category — **objective calibration** — by introducing a novel framework called LiMMo (Linear Meta-Model optimization), which employs a cost-efficient linear regression-based emulator combined with gradient-based optimization.

Previous studies on objective calibration have mainly centred on quadratic regression-based emulators, which permit nonlinear interactions among parameters and offer robust approximations (introduced in Neelin et al. (2010) and utilized in Bellprat et al. (2012, 2015); Avgoustoglou et al. (2022)). However, a key limitation of this method is its high computational cost: the number of simulations required increases with the number of parameters (N) as N^2, since the simulation must be conducted for each pair of disturbed parameters in order to approximate interaction terms. To explore parameter space, many studies have employed Monte Carlo or Latin Hypercube sampling, which requires an exponentially growing number of samples to find global minimum for the error norm function, as dimensionality increases (Morokoff and Caflisch, 1995). Although this method is robust, it is computationally intensive and inefficient, restricting its use to tunings involving only a limited number of parameters – typically no more than seven. These constraints underscore the need for more efficient approximation and optimization approaches.

Another important issue is selecting an appropriate objective function to guide optimization. Although there are many alternatives, including multi-objective and probabilistic formulations, many studies continue to rely on simple metrics, such as root mean square error (RMSE) and/or Pearson correlation coefficient. However, RMSE and Pearson correlation may not capture all aspects of model performance (Liemohn et al., 2021). Nevertheless, to demonstrate the capabilities of the proposed LiMMo framework in a transparent and tractable way, this study focuses on minimizing RMSE. This relatively simple error norm allows us to demonstrate the LiMMo framework's capabilities, laying the groundwork for future expansions to more advanced metrics that take the distribution function into account.

The literature on statistical emulators includes Gaussian process models (Kennedy and O'Hagan, 2001; Williamson et al., 2013), high degree polynomial meta-models (Neelin et al., 2010; Bellprat et al., 2012), and hierarchical emulators that leverage multi-resolution outputs (Williamson et al., 2012). Despite its simplicity, linear regression has received less attention, even though it offers substantial efficiency benefits. Furthermore, gradient-based optimization techniques have rarely been applied to climate model tuning, partly due to the difficulty of computing derivatives. Taking advantage of the structural simplicity of linear regression makes it easier to derive the gradients of the objective function analytically and implement the gradient-based optimization procedure. This improves the scalability and convergence properties of the optimization process. To our knowledge, this is the first application of gradient-based optimization in the context of objective calibration for a regional climate model.

The following text is divided into five sections. The **materials** (section 2) describes the tuned model quantities, the observational data sets, the regional climate model and its physical parameterizations. The tuning method is introduced in section **The LiMMo framework** (section 3). The **results** of the optimization are presented in section 4. **Discussion** in section 5 covers aspects of tuning that fall outside the scope of the current study. Finally, the most important results are highlighted in **conclusions** (section 6).

2 Materials

In this section, we provide a detailed description of ICON-CLM regional climate model (Pham et al., 2021). The model was configured at a 12-km spatial resolution over the EURO-CORDEX domain (Jacob et al., 2014) and optimized against observational data. The list of considered model quantities is presented in section 2.1. Details of the observational data sets are provided in section 2.2. The setup of the regional climate model ICON-CLM is described in section 2.3, while the list of ICON-CLM tuning parameters is outlined in section 2.4.

2.1 Model quantities

The list of surface prognostic variables considered in this study is shown in the Tab. 1.

Table 1. The list of surface model quantities considered in the tuning process.

Acronym	Description	Unit
tas	hourly mean 2-meter temperature	K
rsds	hourly mean downward net short-wave radiation flux	$W \cdot m^{-2}$
tasmin	daily minimum 2-meter temperature	K
tasmax	daily maximum 2-meter temperature	K
psl	hourly mean atmospheric pressure at the surface	Pa
pr_amount	hourly total amount of precipitations	mm per h
hfls	hourly mean surface downward latent heat flux	$W \cdot m^{-2}$

The selection of variables can be adjusted according to the user's interests. In addition to the commonly analyzed variables (**tas**, **tasmin**, **tasmax**, **pr_amount**, **psl**), we include the latent heat flux (**hfls**) due to its significant influence on long-term precipitation formation via evaporation over the sea. These 2D quantities were extracted from both climate model output and observational data sets for the tuning period from January 1, 2003 to December 31, 2008.

2.2 Observational data sets

The E-OBS version 29.0 data set (Cornes et al., 2018) was selected as a reference for **tas**, **rsds**, **tasmin**, **tasmax**, **psl** and **pr_amount**. This land-only, station-based observational gridded data set is compiled from high-density in-situ measurements provided by over 2000 European meteorological and hydrological stations. These measurements are then interpolated onto a regular grid and provided with ensemble uncertainty estimates. It provides high-quality daily data over Europe with a spatial resolution of approximately 25 km (12 km resolution is also available in the latest versions) and temporal coverage since 1950. Due to its fine spatial detail, daily temporal resolution and ensemble-based uncertainty estimates, E-OBS is a robust resource for analysing regional climate variability and long-term trends, and for making reliable climate assessments.

80   Our aim is to calibrate the **hfls** to align with the HOAPS version 4.0 data set (Andersson et al., 2010). HOAPS provides a satellite-based climatology of latent heat flux over the global ice-free oceans, derived from recalibrated SSM/I and SSMIS sensor measurements. The data set covers the period from 1987 to 2014, has a spatial resolution of approximately 55 km, and provides 6-hourly averages. HOAPS uses the COARE bulk flux algorithm version 2.6a (Fairall et al., 2003), to provide accurate estimates, making it a key reference for ocean-atmosphere interaction studies and energy exchange assessments.

85   Temporally averaged surface fields of **tasmin**, **tasmax**, **rsds**, **pr_amount**, **psl**, and **hfls** interpolated to the climate model output grid are shown in Fig.1 for the tuning period 2003-2008.
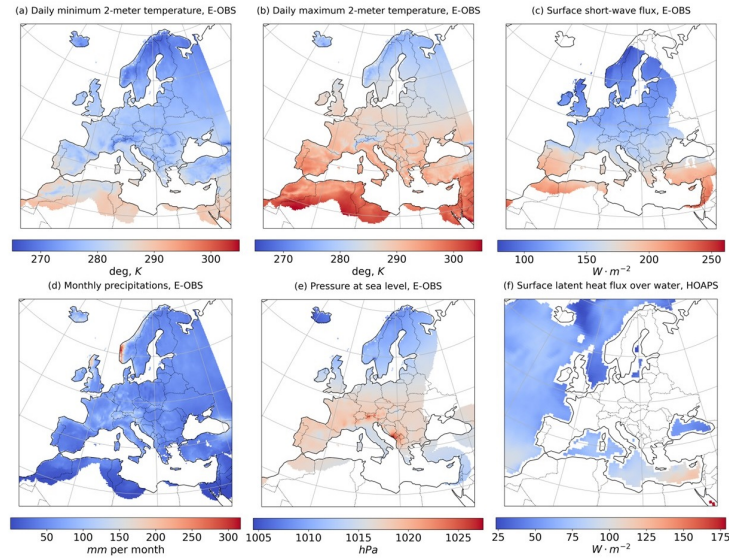

Figure 1. 2003-2008 mean observations: (a) daily minimum 2-meter temperature, E-OBS; (b) daily maximum 2-meter temperature, E-OBS; (c) daily mean short-wave radiation flux, E-OBS; (d) total monthly precipitations, E-OBS; (e) daily mean atmostperic pressure at sea level, E-OBS; (f) daily mean latent heat flux over water, HOAPS.

2.3   Regional climate model ICON-CLM

ICON is a state-of-the-art model for global circulation modeling, Regional Climate Modeling (RCM), operational Numerical Weather Prediction (NWP), Large Eddy Simulations (LES), and environmental prediction (Zängl et al., 2015; Klocke et al., 2017; Stevens et al., 2017). The model is available since 2024. It uses an unstructured triangular grid, allowing nearly uniform resolution across the globe at any grid scale. The model is capable of simulations down to sub-kilometer scales, with common dynamics and numerics across all application modes. The model physics, however, differs between applications, with specific versions for Earth system modeling, NWP/RCM, and LES.

    ICON-CLM (ICON in Climate Limited-area Mode) is the configuration used for RCM applications. It utilizes NWP physics with climate-specific extensions for long-term simulations. The first version of ICON-CLM is based on ICON release 2.6.1

4

(Pham et al., 2021). Typically, it operates in a one-way nesting mode, with coarse grid lateral boundary conditions and bottom boundary conditions over oceans. In the current study, Rayleigh damping is applied at the upper boundary to handle gravity waves.

100   The ICON release model version from 2024.07 (ICON partnership (DWD, MPI-M, DKRZ, KIT, C2SM), 2024) is used with the ERA5 reanalysis (Hersbach et al., 2020) boundary conditions for the period 2003-2008. The simulation grid R13B5 (ICON terminology) corresponds to a mesh size of about 12.14 km. As a post-processing step, the model fields were interpolated onto a rotated 412×424 rectangular grid of the EURO-CORDEX model domain (Fig. 2) with a spatial resolution of 12 km, ensuring convenient data storage and accessibility for analysis.
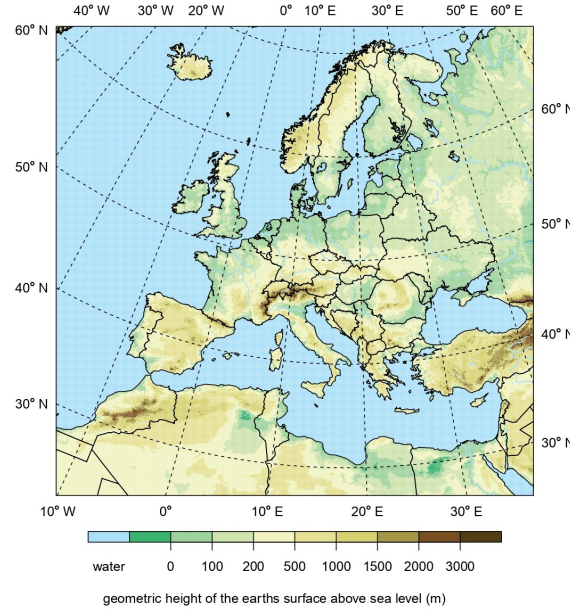

Figure 2. EURO-CORDEX domain, height of the Earths surface above sea level.

2.4   Tuning parameters of ICON-CLM

105   In this study, 15 parameters are selected for optimization, which is twice the number of parameters used in applications of the quadratic regression Meta-Model approach (Bellprat et al., 2012; Avgoustoglou et al., 2022). The following subsections discuss the physical meaning and relevance of these parameters. All model parameters are grouped into four categories. A brief description of the **Surface Transfer Scheme** (section 2.4.1) and **Mixing in the Planetary Boundary Layer** (section 2.4.2) parameters is given in Tab. A1 in the Appendix. Descriptions of the **Cloud Cover** (section 2.4.3) and **External Data sets**

110   (section 2.4.4) parameters can be found in Tab. A2. For more details, please refer to the ICON namelist parameter overview (https://gitlab.dkrz.de/icon/icon-model/-/blob/release-2024.07-public/doc/Namelist_overview.pdf).

The ICON namelist parameter names are designed to be self-explanatory, but this often results in them being quite long. To address this, the tables in the appendix (Tab. A1 and Tab. A2) provide a mapping between the full ICON parameter names and the shorter versions used in the current study. In the text, ICON parameter names are highlighted with `mono-space` font, while the corresponding short acronyms are highlighted with **bold** font. For example, the ICON parameter for the relative humidity range is `tune_box_liq`, which corresponds to the acronym **tbl**.

2.4.1 Surface Transfer Scheme

The surface transfer scheme contains several tuning parameters, some of which are known to significantly impact near-surface climate conditions. These parameters, along with several related and newly introduced ones, are used for optimization. Specifically, the parameters `rlam_heat`, `rat_sea`, `cr_bsmin`, and `rsmin_fac` have been identified as particularly sensitive in climate modeling. Even small changes within their uncertainty ranges can lead to substantial changes in the simulated climate, particularly in the near-surface air temperature (**tas**). These parameters have been optimized in previous studies (Bellprat et al., 2012; Avgoustoglou et al., 2022).

The parameters `rlam_heat` and `rat_sea`, along with the newly introduced parameter `rat_lam`, serve to scale the resistance to latent and sensible heat flux over both land and sea surfaces, as described in the Tab. 2.

Table 2. Influence of the parameters `rlam_heat`, `rat_sea`, and `rat_lam` on the latent and sensible heat fluxes.

	Land	Sea
Latent Heat Flux	`rlam_heat · rat_lam`	`rlam_heat · rat_sea`
Sensible Heat Flux	`rlam_heat`	`rlam_heat · rat_sea`

These parameters provide the flexibility to tune the heat fluxes over land and sea surfaces independently, and allow the adjustment of the Bowen ratio over land surfaces.

The parameters `cr_bsmin` and `rsmin_fac` represent the minimum resistance to evaporation from bare soil, relevant for wet soil conditions, and the scaling factor for the minimum resistance of plant transpiration, respectively. These minimum resistances limit evapotranspiration and are known to have a significant impact on soil moisture. Consequently, they influence the annual cycle climatologies, especially with respect to soil moisture dynamics.

Recently, the parameter pair `tune_albedo_wso` = (**taw1**, **taw2**) was introduced to correct the reference albedo for dry (**taw1**) and wet (**taw2**) soil conditions. This parameterization was initially motivated by the model's warm **tas** bias in the Mediterranean and cold bias in central and northern Europe. Additionally, it accounts for the fact that observed albedo tends to be reduced for wet soils and increased for very dry soils.

2.4.2 Mixing in the Planetary Boundary Layer

The parameters `tkhmin` and `tkmmin` represent the minimum diffusion coefficients for vertical mixing of heat and momentum, respectively. They maintain mixing under opaque cloud cover and help dissolve the clouds, compensating for the excessive

effective viscosity caused by numerical diffusion, which dampens instabilities. However, this minimum diffusion can keep mix-
ing too high in stable, low-turbulence conditions, especially in winter, leading to excessively warm near-surface temperatures.
These parameters should be as low as possible, but high enough to be effective, and have previously been optimized by expert
judgment or objective calibration (Avgoustoglou et al., 2022). In this study, `tkhmin` and `tkmmin` are tuned simultaneously
with the same factor (later the same acronym **tkhmin** is used for `tkhmin = tkmmin`).

2.4.3 Cloud Cover

The cloud cover parameters are optimized to address the **rsds** bias. The `tune_box_liq` and `tune_box_liq_asy` param-
eters are introduced to adjust the relationship between cloud cover (CLC) and relative humidity (RH), and are carefully tuned
for operational NWP applications.

The `allow_overcast` factor further refines the dependence of cloud cover on relative humidity. Values less than one in-
crease the average cloud cover. To incorporate seasonal variability, we define a time-dependent monthly variation for `allow_overcast`
as follows:

$$\texttt{allow\_overcast}[i] = \mathbf{ao} + \mathbf{aot4} \cdot aot[i],$$

where **ao** is the mean and $aot[i]$ are the monthly deviations from that mean, i is the index of the month. The deviations are
predefined to be positive in summer and negative in winter. This monthly variability is parameterized in the Meta-Model by
the mean (**ao**) and the scaling factor ($0.0 \leq \mathbf{aot4} \leq 1.5$) of the monthly deviations.

2.4.4 External data sets

In recent years, new data sets describing the physical properties of soils, surfaces, and the atmosphere have become available.
In this study, we investigate the following alternative options:

- `soil_data_base` (**sdb**) describes the physical properties of the soil, provided by FAO (FAO/UNESCO, 1981) [**sdb** = 0]
  and HWSD data (Nachtergaele et al., 2023) [**sdb** = 1]. The FAO data set mainly represents sandy soils with a typical
  spatial resolution of 50 km, while the HWSD data set has a finer resolution of approximately 7 km.

- `type_of_orography` (**oro**) is used to calculate the grid-scale surface elevation and parameters required to parameter-
  ize subgrid-scale orographic effects. We use the global NOAA GLOBE data (GLOBE Task Team et al., 1999) [**oro** = 0]
  with a resolution of 30 arcseconds (approximately 1 km), or the Yamazaki-Lab MERIT data (Yamazaki et al., 2017)
  [**oro** = 1] with a finer grid resolution of 3 arcseconds (approximately 100 meters).

- `type_of_aerosols` (**acrf**) parameterizes the feedback of the Cloud Condensation Nuclei Density (CDNC) on cloud
  formation. For this study, we use Kinne aerosol data (Kinne, 2019) [**acrf** = 0], for which CDNC is not available, so we
  supplement it with MODIS (Schaaf et al., 2021) [**acrf** = 1] CDNC data.

7

3 The LiMMo framework

This section introduces the LiMMo tuning framework. In principle, the described steps are model-independent, enabling users to adopt the framework for their own tuning objectives. The definition of the error norm relative to observations, which serves as the optimization objective, is discussed in section 3.1. The Meta-Model approximation methodology is explained in section 3.2. The proposed gradient-based optimization method is described in section 3.3. Finally, in section 3.4, we introduce the measure of quantity sensitivities with respect to model parameters.

3.1 Error norm

The standard ICON-CLM model output is generated on an hourly basis (except for **tasmin**, **tasmax** which are daily). To reduce the temporal dimensionality, the daily means for **tas**, **rsds**, **psl**, and **hfls** and the daily sum for **pr_amount** are computed first. To maintain temporal consistency across analyses, an annual cycle of daily values was generated, based on multi-year daily means for each model variable. This approach allows for flexibility in the selection of time spans per variable to accommodate any temporal inconsistencies in observations. For this study, a uniform six-year period from 2003 to 2008 was used across all variables for both model outputs and observations to generate the annual cycle. In addition, to further reduce the dimensionality of the data, monthly mean values of the annual cycle were calculated for each model variable, consolidating the temporal dimension to 12. In principle, there is no need to accumulate the daily values first to generate the monthly averages of the annual cycles, since one can compute the monthly averages first and then compute the multi-year average of the annual cycle. However, this approach generally provides more flexibility, since it allows for more sophisticated distribution-based monthly quantities (e.g., 99th percentiles of hourly/daily values within climatological month).

To define the error norm we consider horizontal model results $\mathrm{MOD}_{i,j,k,n}$ for variables v_n. The indices i, j correspond to horizontal surface spatial dimensions, k is the index of month. The observational data $\mathrm{OBS}_{i,j,k,n}$ were then interpolated to the model grid.

The spatially reduced Root Mean Square Error $\mathrm{RMSE}_{k,n}$ for each variable and time period is defined as

$$\mathrm{RMSE}_{k,n} = \sqrt{\frac{1}{N_x \cdot N_y} \sum_{i,j} \left(\mathrm{MOD}_{i,j,k,n} - \mathrm{OBS}_{i,j,k,n}\right)^2}, \tag{1}$$

where $N_x \times N_y$ is the number of horizontal grid points of the simulation domain excluding the lateral boundary relaxation zone. For each variable and month the internal variability (or intrinsic uncertainty) $\sigma_{k,n}$ is defined as the RMSE between the reference and disturbance simulation, where the initial conditions were shifted to 1 month

$$\sigma_{k,n} = \sqrt{\frac{1}{N_x \cdot N_y} \sum_{i,j} \left(\mathrm{MOD}^{\mathrm{ref}}_{i,j,k,n} - \mathrm{MOD}^{\mathrm{dis}}_{i,j,k,n}\right)^2}. \tag{2}$$

In order to obtain a reliable measure of the intrinsic uncertainty of the model, both the reference and disturbance simulations should cover a sufficiently long period, as is the case in the current study with a 6-year period. Otherwise, significant imbalances in the monthly values within the climatological year can occur. The unit less error ERR_n for each variable is defined as the

averaged over time periods RMSE error normalized on internal variability

$$\text{ERR}_n = \frac{1}{N_t} \sum_k \frac{\text{RMSE}_{k,n}}{\sigma_{k,n}}, \tag{3}$$

where $N_t = 12$ is the number of months. The final error norm ERR is defined as the weighted sum of the errors for each variable

$$\text{ERR} = \sum_n c_n \cdot \text{ERR}_n, \ \sum_n c_n = 1. \tag{4}$$

The weights c_n are specified by the user to emphasize the importance of a particular variable and should have the unit sum. The goal of the tuning process is to minimize the error norm (Eq. 4) with respect to the model parameters.

3.2 The linear Meta-Model approximation

The mean climate can be regarded as a balanced, stable stationary state and thus to be weakly dependent on the model parameters p_i. This allows to consider the climate state CLI as a function of a model parameter vector $\boldsymbol{p}$ and to expand $\text{CLI}(\boldsymbol{p})$ in a Taylor series around the reference model solution $\text{CLI}(\boldsymbol{p_0})$. The linear meta model is the first order approximation of the climate state:

$$\text{CLI}(\boldsymbol{p}) \approx \text{CLI}(\boldsymbol{p_0}) + \nabla_{\boldsymbol{p}}\text{CLI}(\boldsymbol{p_0}) \cdot (\boldsymbol{p} - \boldsymbol{p_0}). \tag{5}$$

We rewrite Eq. 5 in the form of a linear regression $\text{REG}_{i,j,k,n}$ for each grid point (x_i, y_j), month m_k and variable v_n

$$\text{REG}_{i,j,k,n}(\boldsymbol{p}) = \text{A}_{i,j,k,n} + \sum_{m=1}^{N_c} p_m \cdot \text{K}_{i,j,k,n}^m, \tag{6}$$

where $\text{A}_{i,j,k,n}$ is the shift tensor, $\text{K}_{i,j,k,n}^m$ is the tendency tensor (m is the index of the parameter) and N_c is the number of continuous parameters considered.

To train the linear regression model we present the analytical values of a tendency tensor $\text{K}_{i,j,k,n}^m$ for each m, obtained by the method of undefined coefficients by substituting simulations to the general form of linear regression (Eq. 6). After substituting the reference and single parameter disturbance simulation, the value of the tendency tensor is defined as the fraction of the simulation difference to the parameter increment. For example, one can obtain the tensor $\text{K}_{i,j,k,n}^m$ corresponding to the parameter p_m as

$$\text{K}_{i,j,k,n}^m = \frac{\text{MOD}_{i,j,k,n}^{p_m=p_m^{\text{ref}}+\Delta p_m} - \text{MOD}_{i,j,k,n}^{p_m=p_m^{\text{ref}}}}{\Delta p_m}, \tag{7}$$

since the other parameters except p_m remained unchanged. If more than one linear combination could define the tendency on the parameter, the least-square technique is utilized. The specific values of the parameters used for training (tested values) can be found in Tab.A1 and Tab.A2. After the computation of all tendency tensors, the additional substitution of the reference simulation gives the value of the shift tensor

$$\text{A}_{i,j,k,n} = \text{MOD}_{i,j,k,n}^{\text{ref}} - \sum_{m=1}^{N_c} p_m^{\text{ref}} \cdot \text{K}_{i,j,k,n}^m. \tag{8}$$

To account for logical switches, we incorporate constant signals into the Meta-Model (Eq. 6):

$$\text{REG}_{i,j,k,n}(\boldsymbol{p}) = \text{A}_{i,j,k,n} + \sum_{m=1}^{N_c} p_m \cdot \text{K}_{i,j,k,n}^m + \sum_{l=1}^{N_b} p_l \cdot \left(\text{MOD}_{i,j,k,n}^{p_l=1} - \text{MOD}_{i,j,k,n}^{p_l=0} \right), \tag{9}$$

where N_b denotes the number of binary (logical) parameters, and each binary parameter p_l can take the values 0 or 1. The reference simulation assumes $p_l = 0$ for all binary parameters. When $p_l = 0$, the logical switch is off, and no additional signal is added, so the Meta-Model would reproduce the state of the reference simulation. The inclusion of binary parameters introduces constant shifts in the emulator, but does not affect the gradient of the Meta-Model with respect to continuous parameters. Consequently, **minimization involves only continuous parameters, while logical ones are prescribed to 0 or 1**.

3.3 The gradient-based optimization

The core concept behind Meta-Model tuning is to replace the climate model output with a regression approximation in the definition of the error norm (Eq. 4). Due to the simplicity of the Meta-Model, the gradient of the error norm with respect to the model parameters can be computed analytically. The linear regression approximation (Eq. 9) provides the following analytical expression for the gradient with respect to the continuous parameters:

$$\left(\frac{\partial \text{REG}}{\partial \boldsymbol{p}} \right)_m = \text{K}_{i,j,k,n}^m. \tag{10}$$

Using the chain rule, the analytical form of the gradient of the error norm (Eq. 4) could be written as

$$\left(\frac{\partial \text{ERR}}{\partial \boldsymbol{p}} \right)_m = \sum_n c_n \frac{1}{N_t \cdot N_x \cdot N_y} \sum_k \frac{1}{\sigma_{k,n} \cdot \text{RMSE}_{k,n}(\boldsymbol{p})} \cdot \sum_{i,j} \left(\text{REG}_{i,j,k,n}(\boldsymbol{p}) - \text{OBS}_{i,j,k,n} \right) \cdot \text{K}_{i,j,k,n}^m. \tag{11}$$

The computation of the gradient requires one loop over grid points (i, j), time (k), and model variables (n), making its duration comparable to that of a single norm evaluation $O(N_x \cdot N_y \cdot N_t \cdot N_{\text{vars}})$.

The availability of a fast gradient computation procedure allows the use of different optimization methods. Gradient-descent-type optimization involves iterations over the vector of parameters $\boldsymbol{p}$ that search for the minimum error norm function (Eq. 4) in the direction opposite the gradient (Eq. 11).

This study proposes the implementation of the Limited-memory Broyden-Fletcher-Goldfarb-Shanno with Box constraints (L-BFGS-B) algorithm (Broyden, 1970; Byrd et al., 1995). This method is chosen due to its high convergence speed, being a quasi-Newton method that approximates the Hessian matrix, and its capability to impose constraints on parameter ranges, thereby eliminating nonphysical parameter values during the optimization.

In gradient-based optimization, parameter normalization is highly beneficial, as it results in a spherical shape of isolines, improving the convergence rate by avoiding the steep slopes of the objective function

$$p_i^{\text{new}} = \frac{p_i^{\text{old}} - p_i^{\text{min}}}{p_i^{\text{max}} - p_i^{\text{min}}}. \tag{12}$$

The parameter ranges $p_i^{\text{min}}/p_i^{\text{max}}$ are user-defined (Tab. A1 and Tab. A2) and are used for parameter normalization as well as for the box constraints in L-BFGS-B optimization. Applying this linear transformation to the parameters results in the

10

255 following transformation of the gradient function

$$\left(\frac{\partial}{\partial \boldsymbol{p}} f(p_1^{\text{new}}, ..., p_m^{\text{new}})\right)_i = \left(p_i^{\text{max}} - p_i^{\text{min}}\right) \cdot \left(\frac{\partial}{\partial \boldsymbol{p}} f(p_1^{\text{old}}, ..., p_m^{\text{old}})\right)_i.$$

Fig. 3 illustrates the difference in convergence of the proposed method with and without parameter normalization for a specific parameter configuration. The results clearly demonstrate that the normalized approach achieves the same objective function value, but with an order of magnitude fewer iterations (the objective function decrement was set to 10^{-5} as the stop criterion in both cases).
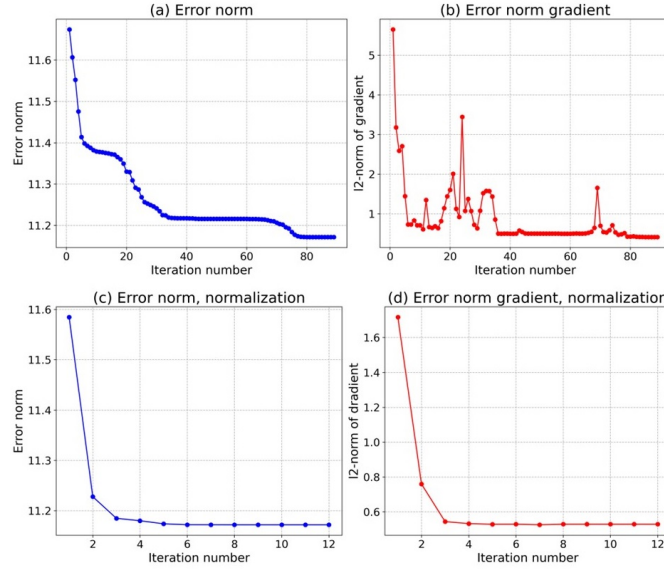
Figure 3. Convergence of L-BFGS-B method: error norm (Eq. 4) values without (a) and with (c) parameter normalization, l2-norm of error norm gradient gradient (Eq. 11) without (b) and with (d) parameter normalization.

260

The dependence of the solution on the initial conditions can lead to different optimization results. An extremely high optimization speed makes it possible to consider the ensemble of optimization trajectories with the perturbed initial conditions. We propose to select the perturbed initial conditions from the Latin Hypercube vicinity of the reference parameters

$$\left[p_m^{\text{ref}} - \textbf{AMPL} \cdot (p_m^{\text{max}} - p_m^{\text{min}}), \; p_m^{\text{ref}} + \textbf{AMPL} \cdot (p_m^{\text{max}} - p_m^{\text{min}})\right], \; m = \overline{1, N_c}. \tag{13}$$

265 The scaling factor $\textbf{AMPL} \in [0, 1]$ defines the amplitude of the perturbation. In the case of the linear regression emulator with a simple RMSE score function, we found no dependence of the result on the initial conditions, as shown in Fig. 4 (we used $\textbf{AMPL} = 0.3$ and 15 samples), but this may be different for more advanced statistical emulators or error norm definitions. If a dependence on the initial conditions occurs, one could choose the result with the minimum value of the objective function.

Gradient-based optimization with an analytical representation of the gradient is highly advantageous in terms of perfor-
270 mance. The use of linear regression as the statistical emulator results in a linear scaling of the dimensions of the problem
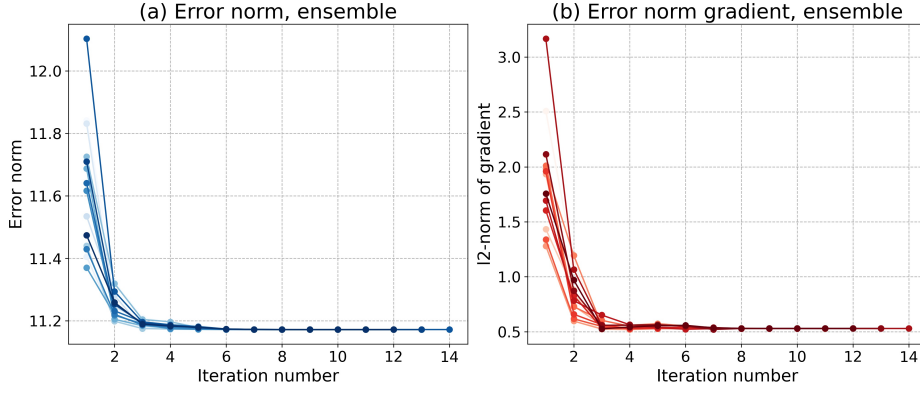
11

Figure 4. The axes are the same as in Fig. 3. Ensemble of 15 optimization trajectories with disturbed initial conditions: (a) error norm (Eq. 4), (b) l2-norm of error norm gradient (Eq. 11).

(number of variables, parameters, grid points, and time steps), allowing a large number of parameters to be tuned in a reasonable amount of time. The numerical approximation of the gradient is also possible in the case of a more sophisticated statistical emulator or an error norm definition when the analytical expression is not available.

3.4 Sensitivity measure

275   To estimate the sensitivity of the ICON-CLM and consequently of the regression model to the considered parameters, the unit-less measure of maximum change $\text{SENS}_{n,m}$ is calculated for each prognostic variable. Firstly we compute the maximal function increments by separately changing all parameters to their limits

$$\Delta\text{REG}_{i,j,k,n}^{m,\min/\max} = \text{REG}_{i,j,k,n}\left(p_1^{\text{ref}}, ..., p_m^{\min/\max}, ..., p_{N_p}^{\text{ref}}\right) - \text{REG}_{i,j,k,n}\left(p_1^{\text{ref}}, ..., p_m^{\text{ref}}, ..., p_{N_p}^{\text{ref}}\right), \tag{14}$$

where N_p is the total number of parameters, including continuous and logical ones. Here, $\Delta\text{REG}_{i,j,k,n}^{m,\min}$ is the regression
280   increment where only the parameter p_m is changed to its minimum limit. Similarly $\Delta\text{REG}_{i,j,k,n}^{m,\max}$ corresponds to the regression increment when p_m is changed to its maximum. The sensitivity benchmark $\text{SENS}_{n,m}$ of the variable v_n to the parameter p_m is defined as the maximum of the sensitivities revealed for $p_m = p_m^{\min}$ and $p_m = p_m^{\max}$ respectively

$$\text{SENS}_{n,m} = \max\left(\text{SENS}_{n,m}^{\min}, \ \text{SENS}_{n,m}^{\max}\right). \tag{15}$$

Eq. 16 gives the expression for calculating the $\text{SENS}_{n,m}^{\min}$ and $\text{SENS}_{n,m}^{\max}$ as the monthly mean signal-to-noise measures (nor-
285   malized by internal variability $\sigma_{k,n}$) of regression increment where $p_m = p_m^{\min}$ and $p_m = p_m^{\max}$ respectively (Eq. 14)

$$\text{SENS}_{n,m}^{\min/\max} = \frac{1}{N_T} \cdot \sum_k \frac{1}{\sigma_{k,n}} \cdot \sqrt{\frac{1}{N_x \cdot N_y} \cdot \sum_{i,j}\left(\Delta\text{REG}_{i,j,k,n}^{m,\min/\max}\right)^2}. \tag{16}$$

12

4   Results

In this section, we analyze the sensitivity results (section 4.1) and the regression validation (section 4.2) to identify the most influential parameters and to evaluate the performance of the proposed statistical emulator. Subsequently, an example applica-290 tion of LiMMo is presented for a selected parameter set (section 4.3), demonstrating its flexibility in handling varying variable weights. Additionally, the results of an optimization incorporating logical switches (section 4.4) constraints are discussed.

4.1   Sensitivity results

The sensitivity measures for all parameters computed as Eq.15 are shown in Fig. 5.

	tas	rsds	tasmin	tasmax	psl	pr_amount	hfls	Avg
taw1	7.235	2.940	5.190	6.683	3.473	1.838	2.235	4.228
taw2	0.730	0.842	0.742	0.739	0.784	0.940	0.937	0.816
rlh	2.047	1.447	2.173	2.060	2.410	1.711	5.067	2.416
rs	2.561	2.218	2.778	2.270	3.061	2.767	6.156	3.116
rl	1.761	2.577	1.837	1.809	1.749	2.132	2.145	2.001
rsmf	2.163	2.268	2.069	2.247	2.032	2.441	2.530	2.250
crb	1.668	1.328	1.576	1.682	1.269	1.445	1.698	1.524
tbl	2.694	6.281	2.733	3.019	3.143	2.595	3.018	3.355
tbla	2.329	5.797	2.100	2.811	2.835	1.733	2.318	2.846
ao	3.826	7.540	2.723	4.281	3.524	2.266	3.232	3.913
aot4	2.179	3.241	1.761	2.274	1.590	1.590	2.016	2.093
tkhmin	2.571	1.203	3.416	1.760	1.366	1.306	1.342	1.852
sdb	2.358	0.833	4.093	1.434	0.925	0.984	1.666	1.756
acrf	0.954	1.249	0.917	0.973	0.940	0.997	0.942	0.996
oro	1.794	0.903	1.968	1.448	1.272	1.110	1.455	1.421

Figure 5. The sensitivity measure of prognostic variables (columns) on model parameters (rows) computed as Eq. 15. The 'Avg' column shows the mean sensitivity of the model to the parameter, calculated as the mean values in the rows. Darker shades are used to color the background of the numbers for larger values.

Overall, the sensitivity results are consistent with theoretical expectations. It is clear that the surface albedo parameterisation 295 **taw1** is the primary driver of surface air temperature variations (**tas**, **tasmin**, **tasmax**). **taw2** has a negligible impact on the model variables, which is below the level of the ICON-CLM's intrinsic variability. The heat flux scaling factors **rlh** and **rs** show sensitivity primarily to latent heat flux over the sea (**hfls**), with a moderate impact on other quantities. The ratio of the laminar scaling factors **rl** has the greatest impact on short-wave radiation (**rsds**), contributing only slightly to precipitation (**pr_amount**) and latent heat flux (**hfls**). The soil resistance parameters **rsmf** and **crb** exhibit sensitivity across all model variables. Although 300 optimizing these parameters may not lead to improvements in one variable without affecting others, their inclusion may still be beneficial for optimization.

13

The cloud cover parameters **tbl** and **tbla** and the allow overcast parameterization **ao** and **aot4** demonstrate the most pronounced sensitivity to short-wave radiation (**rsds**), as expected. The momentum and vertical diffusion coefficient **tkhmin** primarily influence the mean (**tas**) and the minimum (**tasmin**) daily temperature with minimal impact on other variables, suggesting opportunities for targeted tuning.

The external soil database **sdb** primarily affects the mean (**tas**) and the minimum (**tasmin**) daily temperature. Aerosol type **acrf** has only a limited effect on short-wave radiation (**rsds**). The orography type **oro** has a small effect on all model variables, although it is known to influence wind speed, which is outside the scope of this study.

The proposed sensitivity measure is highly effective for evaluating the impact of parameter changes on model variables and for comparing these impacts quantitatively. This analysis is particularly valuable when considering new parameters, as it helps to assess their influence on model results. Parameters that have a low sensitivity across all model variables (less than 1) could either be removed from the optimization or have the limits of their variation expanded.

4.2 Meta-Model validation

Several parameter configurations were additionally simulated with ICON-CLM to evaluate the accuracy of the linear Meta-Model approximation. Due to limited computational resources, only a subset of parameters was considered. The most influential parameters, which exhibited the largest sensitivity in the sensitivity analysis (see Fig. 5), were selected: **taw1**, **rlh**, **rs**, **rl**, **tbl**, **tbla**, **ao** and **tkhmin**. Test samples were generated by simultaneously varying these parameters from the Latin Hypercube within the intervals from minimum to maximum values (see Tab. A1 and Tab. A2).

A direct comparison between the regression model and the ICON-CLM simulation for different grid points and months is presented in Fig. 6. Here values are plotted together for all test cases from Latin Hypercube. For the variables **tas**, **tasmin**, **tasmax**, **psl**, and **hfls**, the coefficient of determination (R^2) exceeds 0.95 (not shown), indicating a decent approximation by the linear model. The variable **rsds** exhibits some spread around the mean, but maintains a high determination coefficient(> 0.99). The precipitation (**pr_amount**) shows the poorest performance of all optimization variables. The spread exhibits values of up to 100 mm per month and the determination coefficient R^2 is 0.9 only. A comparison of the histograms (not shown) reveals that the Meta-Model yields slightly higher precipitation values than ICON-CLM. Also, due to the lack of physical constraints, the Meta-Model yields marginally negative precipitation values; however, their impact on the overall RMSE is very limited (approximately 3% of the intrinsic uncertainty of precipitation (Eq. 2)).

To assess the inaccuracy of the approximation statistically, we computed the monthly mean values of RMSE between the ICON-CLM output and the linear Meta-Model for each test case in the Latin Hypercube, and plotted the mean values in Fig. 7. As can be seen, the imprecision of the linear approximation (green bars) is slightly greater than the intrinsic uncertainty of the ICON-CLM (orange bars), by a factor of 1.5–1.7 for **tas**, **rsds**, **tasmin**, **tasmax** and **pr amount**, and by a factor of 2.5 for **hfls**. However, this imprecision (green bars) is still much smaller than the typical error to observations (blue bars) for all variables except precipitation, indicating the potential for optimization.

The linear approximation error for various variables was also assessed by comparing the time-averaged (averaged over all climatological months) RMSEs to the observations (Eq.1), as shown in Fig.8. For each of the Latin Hypercube validation
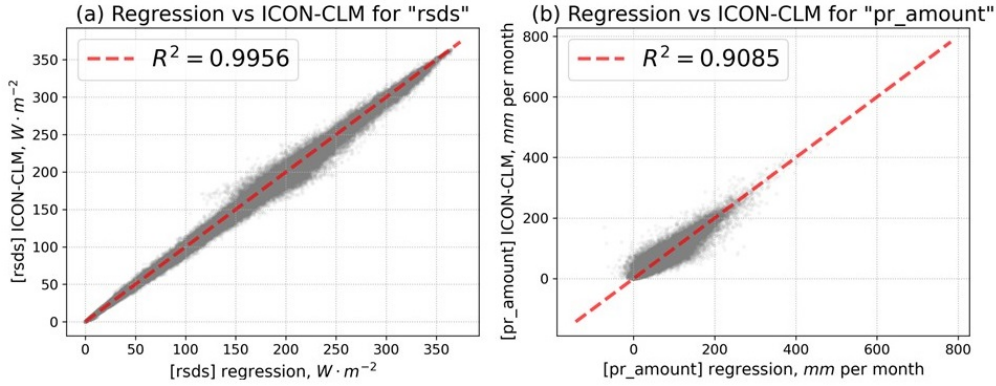
Figure 6. Regression vs. ICON-CLM for the variables **rsds** (a) and **pr_amount** (b). Each grey point shows the monthly value of the model quantity for a single grid point in the model domain, for one of the validation configurations (i.e., all validation cases plotted together). The dashed red line indicates "perfect match", the value of the R2 determination coefficient is given in the label. Every 100th grid point is shown in the plot.
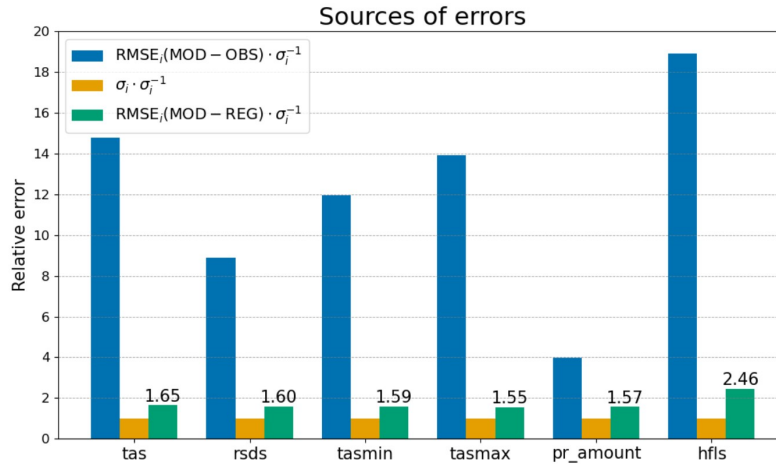

Figure 7. The comparison of the different sources of error in LiMMo. Values are normalized on the intrinsic variability σ_i of the ICON-CLM (Eq.2) for each model variable. The blue bar shows the RMSE of the ICON-CLM output with the NWP configuration to the observations. The orange bar shows the intrinsic variability. The green bar shows the RMSE between the ICON-CLM and the linear regression approximation, averaged over all test cases from Latin Hypercube. The temporally averaged values (averaged for all months) are displayed for all quantities.

setups, we plot the RMSE to observations for different pairs of variables, for both the linear regression approximation and the corresponding dynamical simulation. The scores of the dynamical simulations and their corresponding Meta-Model approximations are represented by markers of identical shape. With a few exceptions, the order of the RMSEs for the linear and dynamic models is largely maintained, i.e., if the RMSE is smaller for the regression results, the same is true for the dynami-

15

340   cal simulation. This justifies the reduction in the RMSE-based error norm for the linear emulator, which is minimized by the optimization procedure, corresponding to an improved dynamic setup with reduced biases. This is particularly true when the reduction in RMSE exceeds the level of imprecision in the approximation, bearing in mind the error in the linear approximation.

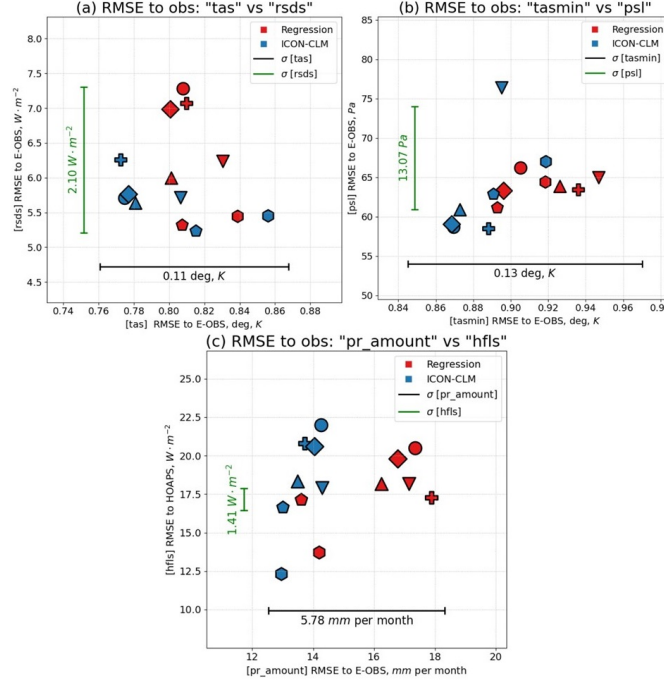This analysis demonstrates the applicability and reliability of the linear approach for representing the dynamical simulations.

Figure 8. The monthly mean RMSEs (Eq. 1) to observations for ICON-CLM simulations (blue markers) and corresponding regression results (red markers) for all parameter setups from Latin Hypercube. Corresponding dynamical and linear setups are indicated by the same marker shape. The 2003-2008 monthly mean RMSEs are shown for: (a) daily mean 2-meter temperature **tas** versus daily mean short-wave flux **rsds**, (b) daily minimum 2-meter temperature **tasmin** versus daily mean sea level pressure **psl**, (c) monthly total precipitation **pr_amount** versus daily mean latent heat flux **hfls**. The 2003-2008 mean internal variabilities of the model (Eq. 2) are shown as horizontal and vertical segments.

4.3   Tuning of continuous parameters

345   LiMMo provides substantial flexibility in the selection of regression parameters for optimization as well as in the weighting of model variables. To systematically evaluate its performance, we fix the set of continuous parameters to the following: **ao**, **aot4**, **taw1**, **taw2**, **rlh**, **rs**, **rl**, **rsmf**, **tbl**, **tbla**, **crb**, and **tkhmin**. Four different weight configurations (Tab.3) for the model variables that define the error norm in Eq.4 are analyzed. As the reference configuration, we used the proposed configuration of ICON for NWP, which defines the shift tensor in Eq. 8. The parameter values of the reference configuration can be found in Tab. 4.

350   The first configuration, '**equal_weights**', assigns equal weights to all model variables. LiMMo allows to explore the predictive potential of the climate model for specific fields, therefore, two extreme cases are considered: '**tune_prec**' assigns

weights exclusively to precipitation, neglecting all other variables, while 'tune_temp' distributes weights among **tas**, **tasmin**, and **tasmax**. Finally, the 'expert_weights' configuration reflects weights determined a posteriori by the authors based on an analysis of the optimization results. There are also some objective ways of defining weights, such as entropy weights for multi-criteria decision-making in information theory, which are beyond the scope of the current study. These could be implemented in the LiMMo framework by assigning a variable weight that is inversely proportional to signal-to-noise values of the initial configuration for each model quantity.

Table 3. The list of considered weights in the error norn definition (Eq. 4). Each row represents the set of weights of the model quantities (columns).

	tas	rsds	tasmin	tasmax	pr_amount	psl	hfls
equal_weights	1.0 / 7.0	1.0 / 7.0	1.0 / 7.0	1.0 / 7.0	1.0 / 7.0	1.0 / 7.0	1.0 / 7.0
tune_prec	0.0	0.0	0.0	0.0	1.0	0.0	0.0
tune_temp	0.25	0.0	0.5	0.25	0.0	0.0	0.0
expert_weights	0.15	0.01	0.18	0.15	0.45	0.01	0.05

The performance scores of the model variables (Eq. 3) after optimization are shown in Fig. 9. Note that in the current study we tend to minimize the variable scores (error norms), so the reduced score values demonstrate the better performance. It is evident that the predictability of precipitation is approaching its theoretical limit for the selected set of model parameters, as the optimal score of **pr_amount** in the 'tune_prec' configuration is only slightly ($\sim 2\%$) lower than that of the reference configuration. It is also worth noting that the initial NWP configuration is already very well tuned for precipitation. Conversely, when optimizing only for temperature variables ('tune_temp'), significant error reductions are achievable: a 5% reduction for **tas**, a 12% reduction for **tasmax**, and a 4% reduction for **tasmin**. However, this comes at the cost of a significant imbalance in the surface heat budget, with notable increases in **rsds** (5%) and **hfls** (47%). The quality of **pr_amount** is also badly affected by 15%.

The 'equal_weights' setup demonstrates significant reductions in **rsds** (10%) and **hfls** (25%), but it underperforms the NWP configuration for the key prognostic variables **tas**, **tasmax**, and **pr_amount**. On the other hand, the 'expert_weights' setup achieves comparable performance to the NWP configuration for most variables, with the exception of **rsds** (1-2% worse) and **tasmax** (2-3% worse). In particular, this setup yields significant improvements in the values of **tasmin** (7%) and **hfls** ($\sim 10\%$). Consequently, the 'expert_weights' setup can be considered as a viable alternative to the NWP configuration. The optimal values of the considered parameters are listed in the Tab. 4.

4.4 Optimization with logical switches

This subsection presents the optimization results obtained using the Meta-Model with incorporated logical switches (Eq. 9). The parameter set is fixed as in the previous subsection, with the 'expert_weights' weight configuration applied. The study considers three logical parameters (**sdb**, **acrf** and **oro**), resulting in a total of eight possible optimizations. The continuous
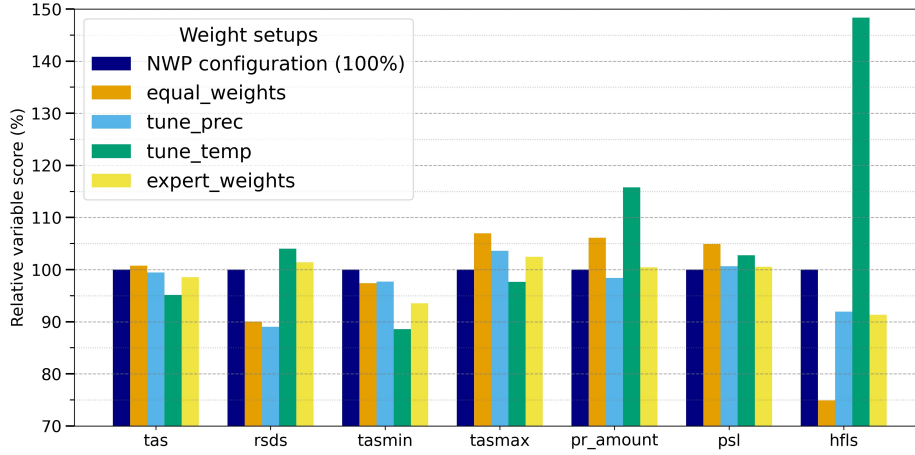
Figure 9. Scores of model variables (Eq. 3) normalized by the variable score of NWP configuration (dark blue bars) after optimization with different weights from Tab.3. Note that in the current study we aim to minimize the variable scores (error norms), so the reduced score values demonstrate the better performance.

Table 4. The parameter values for the ICON-CLM for the NWP configuration and configurations obtained from LiMMo using different weights from Tab. 3. The rows of the table correspond to the different weights of the variables in the optimization, the columns represent the model parameters.

	ao	aot4	taw1	taw2	rlh	rs	rl	rsmf	tbl	tbla	crb	tkhmin
NWP configuration	1.000	0.000	0.000	0.000	10.000	0.800	1.000	1.000	0.050	3.250	110.000	0.600
equal_weights	0.977	0.293	0.044	-0.027	12.000	1.172	0.972	1.082	0.067	3.277	120.825	0.671
tune_prec	0.966	0.123	0.017	-0.015	11.217	0.877	0.969	1.028	0.053	3.373	111.911	0.572
tune_temp	0.980	0.819	0.114	-0.103	5.000	0.605	1.089	1.070	0.040	3.147	115.625	0.566
expert_weights	0.984	0.225	0.071	-0.068	10.497	0.934	0.992	1.057	0.051	3.222	123.650	0.618

parameters were optimized for each configuration of logical switches that defines the shifted linear Meta-Model. The results are summarized in Fig. 10. This final scores table provides the comprehensive information needed to select the climate model configuration that best meets the user's priorities and interests.

380   From the Fig.10 one can clearly see the positive effect of more detailed orography on the latent heat flux (**hfls**), as the bias is significantly reduced for all cases when **oro**=1. Overall, updating all external data sets $(\textbf{sdb}, \textbf{acrf}, \textbf{oro}) = (1, 1, 1)$ leads to the most pronounced improvements in precipitation (**pr_amount**) and latent heat flux over sea (**hfls**).

sdb	acrf	oro	tas	rsds	tasmin	tasmax	pr_amount	psl	hfls	Optimal Norm
1	1	1	15.617	9.038	16.376	13.324	4.423	10.556	17.703	10.361
0	0	0	14.666	8.825	11.855	13.813	4.440	10.145	17.485	9.468
0	0	1	14.642	9.208	12.081	13.870	4.291	10.362	16.047	9.381
0	1	0	14.535	8.503	11.757	13.627	4.277	10.099	17.638	9.333
0	1	1	14.507	8.874	11.986	13.679	4.112	10.296	16.169	9.236
1	0	0	14.770	8.741	12.426	13.712	4.296	9.970	18.012	9.530
1	0	1	14.754	9.157	12.668	13.774	4.154	10.212	16.509	9.448
1	1	0	14.657	8.419	12.339	13.540	4.122	9.925	18.159	9.397
1	1	1	14.636	8.822	12.586	13.595	3.963	10.147	16.625	9.304

Figure 10. The variable scores (Eq. 3) for the optimal configurations with different sequences of logical switches. The first row represents the reference NWP configuration. The first three columns describe the sequence of logical switches, while the following columns give the resulting scores for the considered variables. The last column shows the optimal norm (Eq. 4). The values are color-coded with a gradient from red to green, indicating relative deficiency or improvement compared to the corresponding reference values.

5   Discussion

The LiMMo optimization strategy demonstrates significant potential for objective calibration. While it quickly and automatically generates optimal parameter values, it requires extensive expert knowledge of the model parameters. The user must define the parameter set, ensure the sensitivity of model outputs to parameter changes, and determine the optimization objective, which is reflected in the assignment of the error norm. The computational efficiency of LiMMo allows for an extensive definition of the error norm. In this study, seven different model quantities are considered, which is a significant increase compared to previous studies. However, for simplicity, we limit the error norm to mean values (root mean square error). From a methodological perspective, it is feasible to include more sophisticated and critical quantities such as extreme precipitation (e.g., the 99th percentile of hourly precipitation over a given period), the diurnal cycle of precipitation, and/or short-wave radiation. Tuning these quantities will be a focus of future research. The current study investigates 10-15 model parameters simultaneously, a scale that was previously unfeasible. However, the linear scalability of the optimization time with respect to the number of parameters allows for a significant expansion of this range, potentially by hundreds of parameters.

Another important aspect, which is beyond the scope of this study, is the monthly weighting of the model variables in the definition of the error norm (Eq. 3, Eq. 4). Given the broad tuning period of six years, the computation of multi-year averages significantly reduces the imbalance of monthly internal variability (Eq. 2), ensuring that the signal-to-noise ratio is approximately equal across months. Therefore, further reduction of temporal dimensionality by considering monthly averages (Eq. 3) is sufficient to treat all months equally. However, for shorter tuning periods, the monthly imbalance in the signal-to-noise ratio may become more pronounced, especially since climate models typically exhibit greater internal variability during the summer months. In such cases, considering monthly averages could lead to an underestimation of the impact of summer

months on the model quality score. A more general approach would be to introduce monthly weights for variable errors $f_{k,n}$ (where k is the month index, n is the model variable index), so that the final error norm in the optimization would be

$$\text{ERR} = \sum_n c_n \cdot \sum_k f_{k,n} \cdot \frac{\text{RMSE}_{k,n}}{\sigma_{k,n}}; \ \sum_k f_{k,n} = 1.$$

This would allow control over the contribution of monthly errors, allowing the weights $f_{k,n}$ to be adjusted to balance their contribution to the overall error norm. For example, one could choose the monthly weights to be inversely proportional to the signal-to-noise ratio for the reference simulation:

$$f_{i,n} \cdot \frac{\text{RMSE}_{i,n}^{\text{ref}}}{\sigma_{i,n}} = f_{j,n} \cdot \frac{\text{RMSE}_{j,n}^{\text{ref}}}{\sigma_{j,n}}, \ \forall \ i,j; \ \sum_k f_{k,n} = 1.$$

6   Conclusions

The current study introduces a new tool for objective tuning of regional climate models. Building on previous work (Neelin et al., 2010; Bellprat et al., 2012; Avgoustoglou et al., 2022), the LiMMo framework employs a regression-based approximation of climate model outputs. Unlike previous approaches, LiMMo primarily uses a linear regression approximation rather than a quadratic one. This choice is motivated by the cost-effectiveness of building the statistical emulator, as it requires only a linear number of dynamical simulations (at least one for each parameter). Despite its simplicity, the approximation has demonstrated high accuracy when modeling over long periods of time, as evidenced by the 6-year span considered in this study.

A second distinctive feature of LiMMo is the use of a gradient-based method to minimize the error norm relative to observations, in contrast to previously proposed Monte Carlo methods. The combination of a linear Meta-Model with fast gradient-based optimization allows the approach to scale linearly with the number of model quantities and parameters, allowing the simultaneous tuning of dozens of parameters, a task previously infeasible due to time-to-solution constraints.

The LiMMo framework was applied to the state-of-the-art regional climate model ICON-CLM, tuned to the E-OBS and HOAPS observational data sets. A total of 15 model parameters were optimized using 7 model variables that define the distance of the model to the observations. Different optimization objectives were explored by assigning different weights to the model variables in the error norm definition. In addition, optimization was performed for 8 different sequences of 3 logical switches, providing comprehensive insights to select the climate model configuration that best meets the user's priorities.

Please note that the current study is not intended to give any recommendations on the setup of ICON-CLM, but only to demonstrate the capabilities of the proposed LiMMo technique. The final decision of the model configuration should be made after careful and extensive analysis of the model quantities, and LiMMo is only one of the tools that requires expert judgment.

June 2023 (https://doi.org/10.5281/zenodo.10047021, Rockel and Geyer, 2023), which is publicly available on Zenodo; The ICON-CLM simulations were driven by ERA-5 reanalysis data (https://doi.org/10.24381/cds.143582cf, Hersbach et al., 2020, 2017), with optimization performed using the E-OBS (https://doi.org/10.24381/cds.151d3ec6, Cornes et al., 2018; Copernicus Climate Change Service, Climate Data Store, 2020) and HOAPS (https://doi.org/10.24381/cds.92db7fef, Andersson et al., 2010; Copernicus Climate Change Service, 2022) data sets as reference benchmarks; the Python-based LiMMo software tool (version 1.0) is publicly available on Zenodo (https://doi.org/10.5281/zenodo.14662292, Petrov and Will, 2025). This published software package includes the scripts used to generate the plots in the current manuscript.

Appendix A: ICON parameters description

Table A1. The ICON tuning parameters for **Surface Transfer Scheme** (section 2.4.1) and **Mixing in the Planetary Boundary Layer** (section 2.4.2). The section number with description of parameter is given in the column "Section". The "Parameter" column gives the name of the parameter as used in the ICON model, while the "Acronym" column shows the parameter acronym used in this article. The "Type" column indicates whether the parameter is continuous ("C") or binary ("B"). The "Min/Ref/Max" column represent the minimum, reference, and maximum values, respectively. The "Tested values" column shows the values simulated by ICON-CLM, used for regression training. The "Description" column provides a brief explanation of each parameter.

Section	Parameter	Acronym	Type	Min / Ref / Max value	Tested values	Description
2.4.1	`tune_albedo_wso(1)`	**taw1**	C	0.0 / 0.1 / 0.15	0.0, 0.1	Bare soil albedo correction for soil type 3-6 (sand, sandy-loam, loam, clay-loam) and soil water content `w_so` < 0.01.
	`tune_albedo_wso(2)`	**taw2**	C	-0.15 / -0.1 / 0.0	-0.1, 0.0	Bare soil albedo correction for soil type 3-6 (sand, sandy-loam, loam, clay-loam) soil water content `w_so` > 0.02.
	`rlam_heat`	**rlh**	C	5 / 6.25 / 12	6.25, 10.0	Scaling factor of the laminar boundary layer for latent and sensible heat flux. Higher values increase the resistance of reduce the sensible heat flux at the surface.
	`rat_sea`	**rs**	C	0.4 / 0.8 / 1.5	0.4, 0.7	Ratio of laminar scaling factors over sea and land. The larger `rat_sea` the larger the laminar resistance over sea.
	`rat_lam`	**rl**	C	0.7 / 1.0 / 1.3	0.8, 1.0	Ratio of laminar scaling factors of latent and sensible heat flux over land. The larger `rat_lam` the larger the laminar resistance to latent heat flux over land.
	`rsmin_fac`	**rsmf**	C	0.7 / 1.0 / 1.5	1.0, 1.2	Scaling factor of class dependent minimum stomata resistance. This preserves the dependency of the resistance on vegetation type.
	`cr_bsmin`	**crb**	C	80 / 110 / 170	110, 150	Minimum bare soil evaporation resistance (Schulz and Vogel, 2020) if `itype_evsl=5` (`c_soil` if `itype_evsl=2,3,4`).
2.4.2	`tkhmin`	**tkhmin**	C	0.2 / 0.5 / 1.0	0.3, 0.6	Scaling factor for minimum vertical diffusion coefficient for turbulent heat fluxes at the surface. It is proportional to $R_i^{-2/3}$, with R_i Richardson number.
	`tkmmin`	**tkmmin**	C	0.2 / 0.5 / 1.0	0.3, 0.6	As `tkhmin` but for momentum.

Table A2. The ICON tuning parameters for **Cloud cover** (section 2.4.3) and **External data sets** (section 2.4.4). The description of the columns is the same as in Tab. A1.

Section	Parameter	Acronym	Type	Min / Ref / Max value	Tested values	Description
2.4.3	tune_box_liq	**tbl**	C	0.04 / 0.05 / 0.1	0.05, 0.07	Range of relative humidity (RH) for liquid cloud cover (CLC) diagnostics with $1 - \textbf{tbla} \cdot \textbf{tbl} \leq \text{RH} \leq 1 + \textbf{tbl}$. Higher values increase the cloud cover.
	tune_box_liq_asy	**tbla**	C	2.5 / 3.25 / 4.5	3.25, 4	Asymmetry factor for range of RH in liquid cloud cover diagnostics (See tune_box_liq). A smaller value is resulting in a smaller range of CLC increase with RH to 1.
	allow_overcast	**ao**	C	0.8 / 0.9 / 1.0	0.9, 1.0	Parameter of the dependency of CLC on RH. A smaller value is resulting in a steeper CLC(RH) increase to 1.
		aot4	C	0 / 1.0 / 1.5	0.0, 1.0	The amplitude of the annual cycle of monthly deviations of allow_overcast from the mean value of **ao**: $$\text{allow\_overcast}[i] = \textbf{ao} + \textbf{aot4} \cdot aot[i],$$ $$aot = [-0.02, -0.06, -0.03, 0.02,$$ $$0.05, 0.02, 0.02, 0.02,$$ $$-0.02, -0.04, -0.04, -0.03]$$
2.4.4	soil_data_base	**sdb**	B	0.0 / 0.0 / 1.0	0.0, 1.0	Soil type data base. [**sdb** $= 0$]: FAO (FAO/UNESCO, 1981); [**sdb** $= 1$]: HWSD (Nachtergaele et al., 2023).
	type_of_orography	**oro**	B	0.0 / 0.0 / 1.0	0.0, 1.0	Orography data base. [**oro** $= 0$]: NOAA GLOBE 1km resolution (GLOBE Task Team et al., 1999); [**oro** $= 1$]: MERIT 100m resolution (Yamazaki et al., 2017).
	type_of_aerosols	**acrf**	B	0.0 / 0.0 / 1.0	0.0, 1.0	Aerosol climatology data base. [**acrf** $= 0$] Kinne (Kinne, 2019); [**acrf** $= 1$] MODIS (Schaaf et al., 2021).

References

Andersson, A., Fennig, K., Klepp, C., Bakan, S., Graßl, H., and Schulz, J.: The Hamburg Ocean Atmosphere Parameters and Fluxes from Satellite Data – HOAPS-3, Earth System Science Data, v.2, 215-234 (2010), 3, https://doi.org/10.5194/essd-2-215-2010, 2010.

Avgoustoglou, E., Carmona, I., Voudouri, A., Levi, Y., Will, A., and Bettems, J.: Calibration of COSMO model in the Central-Eastern Mediterranean area adjusted over the domains of Greece and Israel, Atmospheric Research, 279, 106 362, https://doi.org/10.1016/j.atmosres.2022.106362, 2022.

Bellprat, O., Kotlarski, S., Lüthi, D., and Schär, C.: Objective calibration of regional climate models, Journal of Geophysical Research: Atmospheres, 117, https://doi.org/10.1029/2012JD018262, 2012.

Bellprat, O., Kotlarski, S., Lüthi, D., Elía, R., Frigon, A., Laprise, R., and Schär, C.: Objective Calibration of Regional Climate Models: Application over Europe and North America, Journal of Climate, 29, 151211135749 001, https://doi.org/10.1175/JCLI-D-15-0302.1, 2015.

Broyden, C. G.: The Convergence of a Class of Double-Rank Minimization Algorithms 2. The New Algorithm, IMA Journal of Applied Mathematics, 6, 222–231, https://doi.org/10.1093/imamat/6.3.222, 1970.

Byrd, R. H., Lu, P., Nocedal, J., and Zhu, C.: A Limited Memory Algorithm for Bound Constrained Optimization, SIAM Journal on Scientific Computing, 16, 1190–1208, https://doi.org/10.1137/0916069, 1995.

Copernicus Climate Change Service: Monthly and 6-hourly total column water vapour over ocean from 1988 to 2020 derived from satellite observations, Copernicus Climate Change Service (C3S) Climate Data Store (CDS), https://doi.org/10.24381/cds.92db7fef, last access: January 2024, 2022.

Copernicus Climate Change Service, Climate Data Store: E-OBS daily gridded meteorological data for Europe from 1950 to present derived from in-situ observations, Copernicus Climate Change Service (C3S) Climate Data Store (CDS), https://doi.org/10.24381/cds.151d3ec6, last access: January 2024, 2020.

Cornes, R., van der Schrier, G., van den Besselaar, E., and Jones, P.: An ensemble version of the E-OBS temperature and precipitation data sets, Journal of Geophysical Research: Atmospheres, 123, 9391–9409, 2018.

Fairall, C. W., Bradley, E. F., Hare, J. E., Grachev, A. A., and Edson, J. B.: Bulk Parameterization of Air–Sea Fluxes: Updates and Verification for the COARE Algorithm, Journal of Climate, 16, 571 – 591, https://doi.org/10.1175/1520-0442(2003)016<0571:BPOASF>2.0.CO;2, 2003.

FAO/UNESCO: Soil Map of the World, 1:5'000'000, https://www.fao.org/soils-portal/soil-survey/soil-maps-and-databases/faounesco-soil-map-of-the-world/en/, last access: March, 2023, 1981.

GLOBE Task Team, Hastings, D. A., Dunbar, P. K., Elphingstone, G. M., Bootz, M., Murakami, H., Maruyama, H., Masaharu, H., Holland, P., Payne, J., Bryant, N. A., Logan, T. L., Muller, J.-P., Schreier, G., and MacDonald, J. S.: The Global Land One-kilometer Base Elevation (GLOBE) Digital Elevation Model, Version 1.0, https://www.ngdc.noaa.gov/mgg/topo/globe.html, last accessed: March, 2023, 1999.

Golaz, J.-C., Horowitz, L. W., and Levy II, H.: Cloud tuning in a coupled climate model: Impact on 20th century warming, Geophysical Research Letters, 40, 2246–2251, https://doi.org/10.1002/grl.50232, 2013.

Hersbach, H., Bell, B., Berrisford, P., Hirahara, S., Horányi, A., Muñoz-Sabater, J., Nicolas, J., Peubey, C., Radu, R., Schepers, D., Simmons, A., Soci, C., Abdalla, S., Abellan, X., Balsamo, G., Bechtold, P., Biavati, G., Bidlot, J., Bonavita, M., De Chiara, G., Dahlgren, P., Dee, D., Diamantakis, M., Dragani, R., Flemming, J., Forbes, R., Fuentes, M., Geer, A., Haimberger, L., Healy, S., Hogan, R., Hólm, E., Janisková, M., Keeley, S., Laloyaux, P., Lopez, P., Lupu, C., Radnoti, G., de Rosnay, P., Rozum, I., Vamborg, F., Villaume, S., and Thépaut, J.-N.:

Fifth generation of ECMWF atmospheric reanalyses of the global climate, Copernicus Climate Change Service (C3S) Data Store (CDS), https://doi.org/10.24381/cds.143582cf, last access: June 2024, 2017.

Hersbach, H., Bell, B., Berrisford, P., Hirahara, S., Horányi, A., Muñoz-Sabater, J., Nicolas, J., Peubey, C., Radu, R., Schepers, D., et al.: The ERA5 global reanalysis, Quarterly Journal of the Royal Meteorological Society, 146, 1999–2049, 2020.

Hourdin, F., Mauritsen, T., Gettelman, A., Golaz, J.-C., Balaji, V., Duan, Q., Folini, D., Ji, D., Klocke, D., Qian, Y., Rauser, F., Rio, C., Tomassini, L., Watanabe, M., and Williamson, D.: The Art and Science of Climate Model Tuning, Bulletin of the American Meteorological Society, 98, 589 – 602, https://doi.org/10.1175/BAMS-D-15-00135.1, 2017.

Hourdin, F., Ferster, B., Deshayes, J., Mignot, J., Musat, I., and Williamson, D.: Toward machine-assisted tuning avoiding the underestimation of uncertainty in climate change projections, Science Advances, 9, eadf2758, https://doi.org/10.1126/sciadv.adf2758, 2023.

ICON partnership (DWD, MPI-M, DKRZ, KIT, C2SM): ICON release 2024.07, World Data Center for Climate (WDCC) at DKRZ, https://doi.org/10.35089/WDCC/IconRelease2024.07, last access: August 2024, 2024.

Jacob, D., Petersen, J., Eggert, B., Alias, A., Christensen, O., Bouwer, L., Braun, A., Colette, A., Déqué, M., Georgievski, G., Georgopoulou, E., Gobiet, A., Menut, L., Nikulin, G., Haensler, A., Hempelmann, N., Jones, C., Keuler, K., Kovats, S., and Yiou, P.: EURO-CORDEX: New high-resolution climate change projections for European impact research, Regional Environmental Change, 14, https://doi.org/10.1007/s10113-013-0499-2, 2014.

Kennedy, M. C. and O'Hagan, A.: Bayesian calibration of computer models, Journal of the Royal Statistical Society: Series B (Statistical Methodology), 63, 425–464, https://doi.org/10.1111/1467-9868.00294, 2001.

Kinne, S.: Aerosol radiative effects with MACv2, Atmospheric Chemistry and Physics, 19, 10 919–10 959, https://doi.org/10.5194/acp-19-10919-2019, 2019.

Klocke, D., Brueck, M., Hohenegger, C., and Stevens, B.: Rediscovery of the doldrums in storm-resolving simulations over the tropical Atlantic, Nature Geosci, 10, 891–896, https://doi.org/10.1038/s41561-017-0005-4, 2017.

Liemohn, M. W., Shane, A. D., Azari, A. R., Petersen, A. K., Swiger, B. M., and Mukhopadhyay, A.: RMSE is not enough: Guidelines to robust data-model comparisons for magnetospheric physics, Journal of Atmospheric and Solar-Terrestrial Physics, 218, 105 624, https://doi.org/10.1016/j.jastp.2021.105624, 2021.

Mauritsen, T. and Roeckner, E.: Tuning the MPI-ESM1.2 Global Climate Model to Improve the Match With Instrumental Record Warming by Lowering Its Climate Sensitivity, Journal of Advances in Modeling Earth Systems, 12, e2019MS002 037, https://doi.org/10.1029/2019MS002037, 2020.

Mauritsen, T., Stevens, B., Roeckner, E., Crueger, T., Esch, M., Giorgetta, M., Haak, H., Jungclaus, J., Klocke, D., Matei, D., Mikolajewicz, U., Notz, D., Pincus, R., Schmidt, H., and Tomassini, L.: Tuning the climate of a global model, Journal of Advances in Modeling Earth Systems, 4, https://doi.org/10.1029/2012MS000154, 2012.

Morokoff, W. J. and Caflisch, R. E.: Quasi-Monte Carlo Integration, Journal of Computational Physics, 122, 218–230, https://doi.org/10.1006/jcph.1995.1209, 1995.

Nachtergaele, F., Velthuizen, H., Verelst, L., Wiberg, D., Henry, M., Chiozza, F., Yigini, Y., Fischer, G., Tramberend, S., Batjes, N., Montanarella, L., Jones, A., Aksoy, E., Boateng, E., and Shi, X.: Harmonized World Soil Database version 2.0, FAO and IIASA, ISBN 978-92-5-137499-3, https://doi.org/10.4060/cc3823en, 2023.

Neelin, J., Bracco, A., Luo, H., McWilliams, J., and Meyerson, J.: Considerations for parameter optimization and sensitivity in climate models, Proceedings of the National Academy of Sciences of the United States of America, 107, 21 349–54, https://doi.org/10.1073/pnas.1015473107, 2010.

Petrov, S. and Will, A.: LiMMo (Linear Meta-Model optimization for regional climate model), Zenodo, https://doi.org/10.5281/zenodo.14662292, last access: January 2025, 2025.

Pham, T. V., Steger, C., Rockel, B., Keuler, K., Kirchner, I., Mertens, M., Rieger, D., Zängl, G., and Früh, B.: ICON in Climate
530   Limited-area Mode (ICON release version 2.6.1): a new regional climate model, Geoscientific Model Development, 14, 985–1005, https://doi.org/10.5194/gmd-14-985-2021, 2021., 2021.

Rockel, B. and Geyer, B.: SPICE (Starter Package for ICON-CLM Experiments), Zenodo, https://doi.org/10.5281/zenodo.10047021, last access: January 2024, 2023.

Schaaf, C., Wang, Z., and Strahler, A.: MODIS/Terra+Aqua BRDF/Albedo Albedo Daily L3 Global 0.05Deg CMG V061, NASA EOSDIS
535   Land Processes Distributed Active Archive Center, https://doi.org/10.5067/MODIS/MCD43C3.061, last accessed: January, 2024, 2021.

Schulz, J.-P. and Vogel, G.: Improving the Processes in the Land Surface Scheme TERRA: Bare Soil Evaporation and Skin Temperature, Atmosphere, 11, https://doi.org/10.3390/atmos11050513, 2020.

Stevens, B., Fiedler, S., Kinne, S., Peters, K., Rast, S., Müsse, J., Smith, S. J., and Mauritsen, T.: MACv2-SP: a parameterization of anthropogenic aerosol optical properties and an associated Twomey effect for use in CMIP6, Geoscientific Model Development, 10, 433–452,
540   https://doi.org/10.5194/gmd-10-433-2017, 2017.

Williamson, D., Goldstein, M., and Blaker, A.: Fast Linked Analyses for Scenario-based Hierarchies, Journal of the Royal Statistical Society: Series C, 61, 665–691, https://doi.org/10.1111/j.1467-9876.2012.01042.x, 2012.

Williamson, D., Goldstein, M., Allison, L., Blaker, A., Challenor, P., Jackson, L., and Yamazaki, K.: History matching for exploring and reducing climate model parameter space using observations and a large perturbed physics ensemble, Climate Dynamics, 41, 1703–1729,
545   https://doi.org/10.1007/s00382-013-1896-4, 2013.

Yamazaki, D., Ikeshima, D., Tawatari, R., Yamaguchi, T., O'Loughlin, F., Neal, J. C., Sampson, C. C., Kanae, S., and Bates, P. D.: A high-accuracy map of global terrain elevations, Geophysical Research Letters, 44, 5844–5853, https://doi.org/10.1002/2017GL072874, 2017.

Zängl, G.: Adaptive tuning of uncertain parameters in a numerical weather prediction model based upon data assimilation, Quarterly Journal
550   of the Royal Meteorological Society, 149, 2861–2880, https://doi.org/10.1002/qj.4535, 2023.

Zängl, G., Reinert, D., Rípodas, P., and Baldauf, M.: The ICON (ICOsahedral Non-hydrostatic) modelling framework of DWD and MPI-M: Description of the non-hydrostatic dynamical core, Quarterly Journal of the Royal Meteorological Society, 141, 563–579, https://doi.org/10.1002/qj.2378, 2015.